CHARACTERIZATION OF CRACKS IN OXIDATION-PROTECTIVE COATINGS

David C. Copley

General Electric Aircraft Engines
Cincinnati, OH 45215

Michael Rooney

Johns Hopkins University
Baltimore, MD 21218
(Formerly with Southern Research Institute)

John R. Koenig

Southern Research Institute
Birmingham, AL 35255

INTRODUCTION

Carbon-carbon materials are being developed for high temperature use in gas turbine engines and other applications. They have high specific strength and stiffness at elevated temperature, as well as thermal shock resistance. Silicon carbide based coatings are commonly used to protect the material from oxidation.

The coating layer, having a higher coefficient of thermal expansion than the substrate, generates tensile thermal stresses during cooldown from processing or operating temperatures, resulting in relief cracking. Thus regular surface crack patterns are a standard feature of the coated composite. At temperatures above the stress-free point, these cracks are closed due to the thermal expansion mismatch, and the coating provides adequate oxidation protection. Additional layers of glass-forming compounds are typically used to protect the substrate in the intermediate temperature range where the cracks have not fully closed. The primary objective of this study was the detection, classification, and characterization of surface cracks, for the purpose of understanding the relation of crack patterns to the material structure.

Conventional fluorescent particle tests are limited by the porosity and irregular surface of the coating layer, which produce an unacceptable background intensity. The differential absorption method was suggested in order to alleviate this problem. Previous applications of the method have been on porous ceramic materials and were quite successful. The test uses fluorescent dye suspended in a carrier fluid which wets the specimen surface. Differences in absorption rate between the coating and substrate preferentially deposit the fluorescent particles near cracks and other defects in the coating layer. Thus cracks which extend through the entire

coating thickness, providing paths for oxidation to occur, should appear more intense than those that are not critical to part performance.

MATERIALS

This work used materials manufactured by the LTV Corporation, consisting of non-inhibited, woven carbon-carbon substrates and a silicon carbide conversion coating with an outer tetraethylorthosilicate (TEOS) surface sealant layer. Test coupons made for the program were 75 by 25 by 6 mm, and were warp-aligned at 0°, 45°, and 90° to the specimen length. Substrate density was nominally 1.6 g/cm^3, with open porosities in the range of 5 to 10 percent. The coatings were between 100 and 600 µm in thickness. The conversion layer was formed by a pack cementation process, and metallography indicated very little porosity in this region. The sealant layer resided almost exclusively on the surface and had a void content approaching 80 percent. Defects were deliberately induced in selected specimens by introduction of grease dots, silicon metal contamination, aluminum pen marks, and release agents during the manufacturing process.

Photomicrographs (Fig. 1) show cracks 5 to 15 µm wide extending completely through the coating layer. Sub-micron width cracks were also found on the surface but rarely penetrated through the coating layer. There were also some interlaminar cracks noted which were presumably generated by shear lag stresses during cooldown.

DIFFERENTIAL ABSORPTION METHOD

Existing dye penetrants consist primarily of suspended particles of random size and shape. Initial trials using these commercially available materials produced images of low contrast; high background intensities were caused by entrapment of sub-micron sized particles in the surface roughness. Further trials, using microencapsulation to provide control of particle size and shape, proved more satisfactory. In the microencapsulation process, fluorescent dyes were dissolved or dispersed in an organic solution of polystyrene (Dow Chemical Type 685D) and the resulting mixture was processed to provide finished microcapsules. The fluorescent dyes were extracted from commercially available Dayglo pigments. Thermogravimetric analysis (TGA) indicated that the microcapsules left no measurable residue after heating to 600°C; this temperature was therefore used to clean specimens between trials.

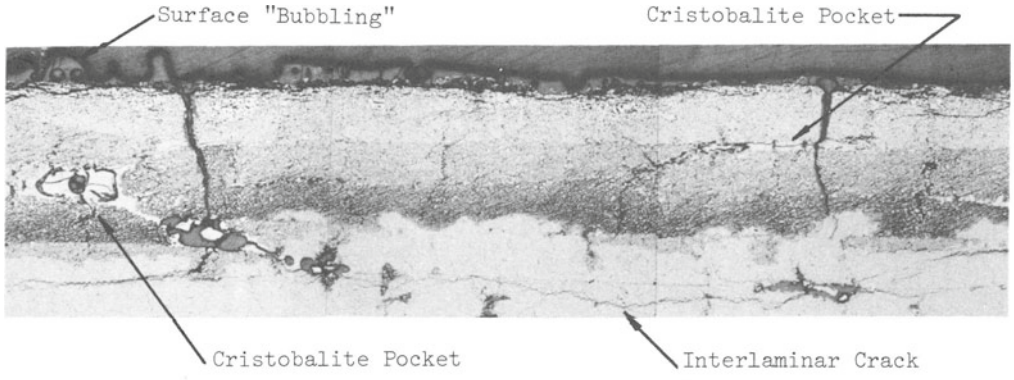

Fig. 1. Cross-section of Coated Carbon-carbon Specimen.

Microcapsules with a size range of 0.5 to 3.0 μm provided the best seating in surface cracks (Fig. 2). Even where there does not initially appear to be total coverage of a crack, the microcapsules can be seen by SEM to be seated down within the crack structure (see Fig. 2 inset). Of the pigments evaluated, Dayglo Blaze Orange provided good contrast under both UV and natural lighting.

The best visibility was obtained from a microcapsule suspension in isopropyl alcohol of 2 grams per liter, agitated prior to application for 15 minutes by an ultrasonic probe to avoid flocculation. Application method was either by dip or spray, and could be varied widely with little effect on crack visibility. A final wash stage was dicontinued because it extracted dye from the cracks (Fig. 3). Specimens were viewed and photographed under a standard blacklight lamp.

This method was performed on all specimens, and regularly spaced crack indications were seen on the faces and edges. Cracks were closely aligned with the warp and fill fiber directions, except near the edges of the 45° specimens. This was consistent with principal stress directions calculated from stress analysis. On a single coupon containing a surface oxidation pit, the cracks radiated from the pit rather than in the warp and fill directions. Wider crack spacings were observed where the coating layer had debonded from the substrate.

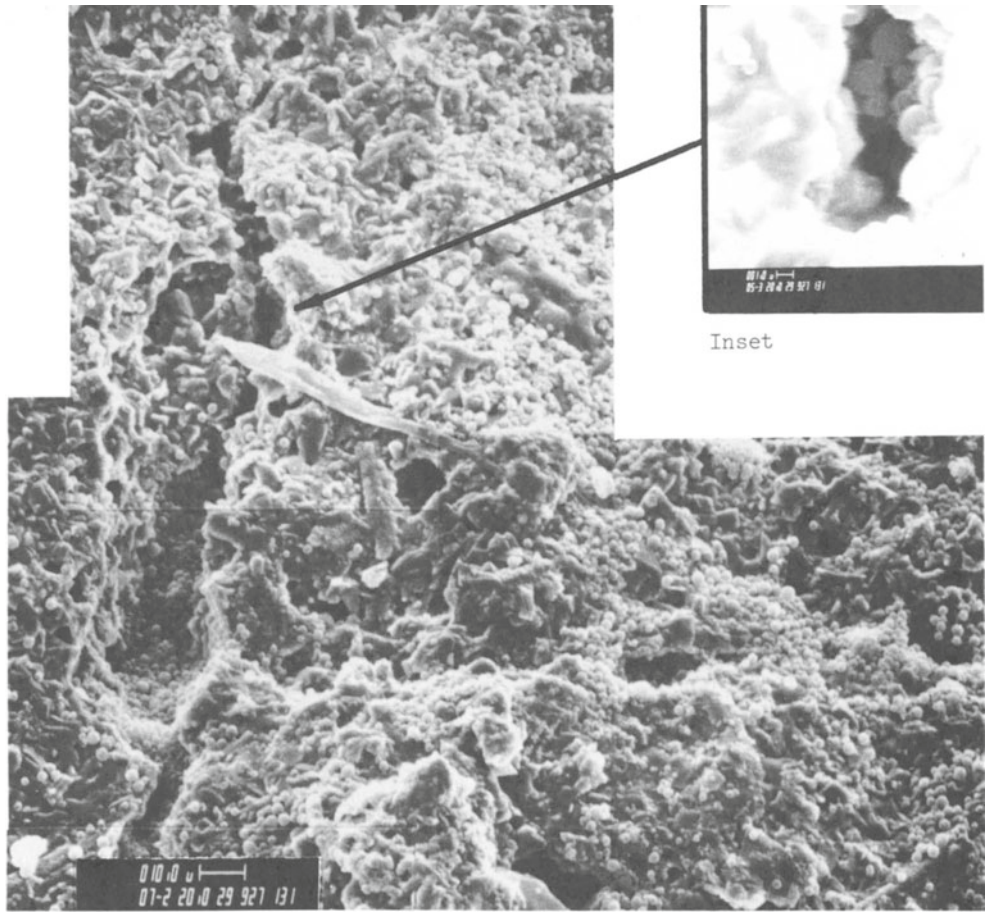

Fig. 2. Seating of Microcapsules in Surface Crack.

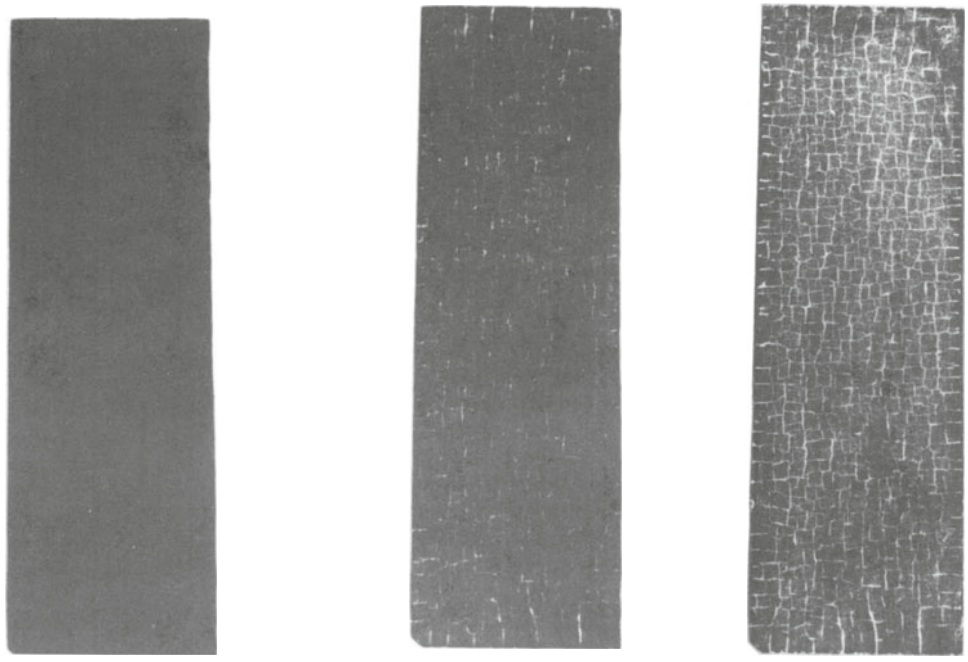

(a) Prior to Dye Application

(b) After Application With Wash

(c) After Application Without Wash

Fig. 3. Effect of Final Wash on Crack Visibility. (Warp-aligned Specimen).

SURFACE FINISH AND OXIDATION EFFECTS

The visibility of crack patterns was related to the thermal exposure of the coupon and the resulting effects on the surface finish. On as-manufactured coupons, cracks were not easily detectable as the final TEOS sealant layer left a rough finish and had partially filled the surface cracks. After the test specimens were held for one hour at 1370°C in air, followed by air cooling to room temperature, the coating surface became glass-like. This reduced the background intensity thus increasing crack visibility. Figs. 4(a)-4(c) show the progression of surface texture with advancing states of oxidation. Final surface condition depended on placement of specimens in the heat treatment oven. Fig. 4(c) shows the bottom surface of a typical oxidized specimen; the surface was in direct contact with fire-brick and thus experienced a lower oxygen flow.

Continued oxidation resulted in total loss of the surface sealant layer. Crack indications were usually more intense in this condition and the crack density was observed to increase in some instances as a result of thermal cycling.

ANALYTICAL APPROACHES

An analytical procedure was developed for modeling the occurrence of cracks in coated carbon-carbon materials. The physical properties used for this study were:

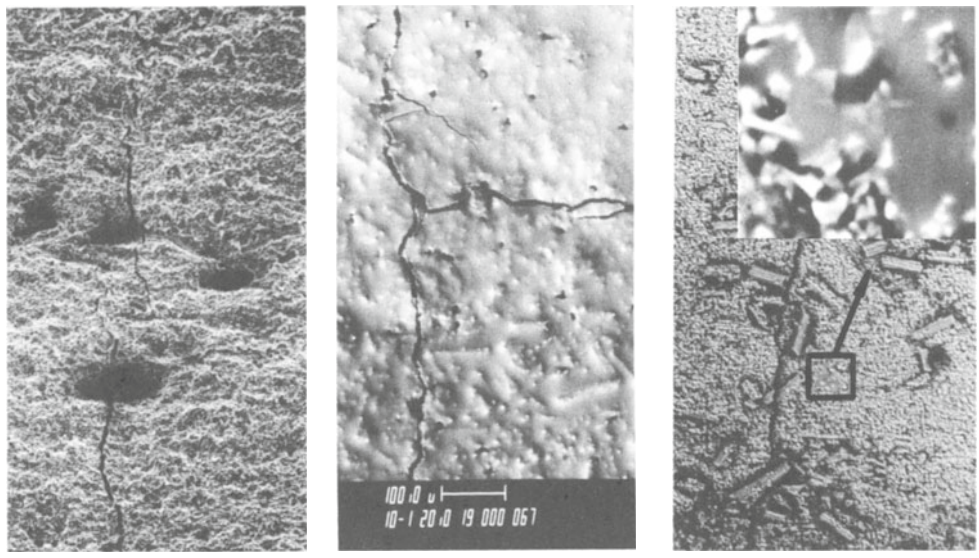

(a) As Received (Dark Areas Represent Surface Charging)

(b) Top Surface after Exposure to 1370°C in Air

(c) Bottom Surface after Exposure to 1370°C in Air

Fig. 4. Surface Alterations due to Thermal Exposure.

Material Property	Coating	Substrate
Density (g/cm^3)	2.59	1.6
Elastic Modulus (GPa)	207	110
Poisson's Ratio	0.19	0.28
Coefficient of Thermal Expansion ($\times 10^{-6}\ K^{-1}$)	5.04	0.9
Allowable Strain to Failure	0.00067	
Stress-Free Temperature (°C)	1315	1315

The classical shear-lag analysis model [1] provided a useful analytical approach for predicting the coating behavior during the temperature cycling. The reducing crack spacing is designated by 2L and was initially taken to be the entire uncracked coating length. Due to the symmetry only the top half of the specimen was modeled. Both the substrate and coating were assumed to be isotropic for the analysis. Using classical shear-lag theory and considering thermal effects, the induced thermal strain in the coating layer was found to be:

$$\varepsilon_{2m} = \varepsilon_o[\cosh(\mu x)/\cosh(\mu L)-1]$$

Where

$$\varepsilon_o = (\alpha_2 - \alpha_1)\Delta T/(1 + E_2h_2/E_1h_1)$$

$$\mu^2 = [G/(h_1 + h_2)][1/E_1h_1 + 1/E_2h_2]$$

$$G = [G_2(h_1 + h_2)]/(h_2 + h_1G_2/G_1)$$

The induced coating strain at the mid-distance between two adjacent cracks is ε_o and $[\cosh(\mu x)/\cosh(\mu L)-1]$ is a strain distribution factor.

The thermally induced strain peaks at the mid-distance between cracks and gradually diminishes toward the cracks. The coefficient of thermal expansion, Young's modulus, shear modulus, and layer thickness are represented by α, E, G, and h, respectively. The subscripts, 1 and 2, denote the substrate and coating materials.

Based on the above equations, the induced thermal strain can be calculated for a specified temperature change, ΔT. If the induced strain exceeds the allowable strain value within an incremental temperature step, a cracking event is assumed to have occurred at the mid-distance between the existing cracks. This incremental process is continued until the specimen reaches its final temperature.

The progressive development of the induced coating strain and crack density for a typical specimen (coating thickness 150 μm) as determined by this model are shown in Figs. 5(a) and 5(b), respectively. A parametric study was conducted by varying the coating thickness and calculating the final crack interval. Fig. 6 shows the prediction of crack spacing as a

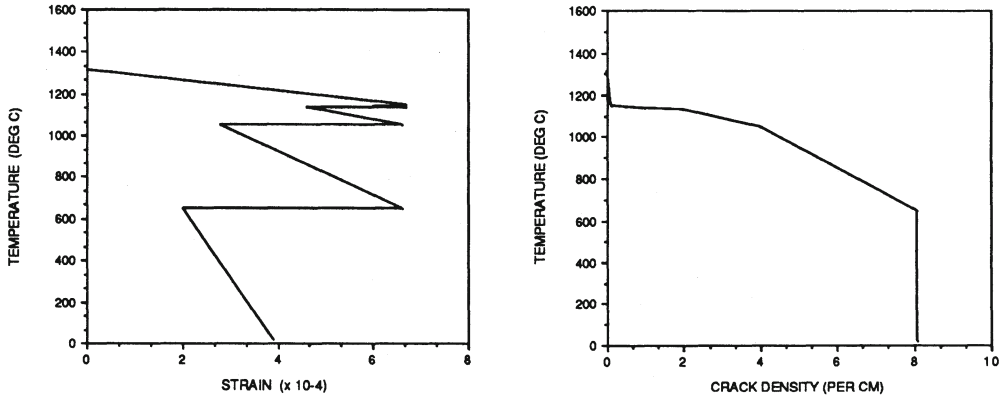

a) Maximum Induced Thermal Strain (b) Crack Density

Fig. 5. Progressive Crack Development on Cooldown from Thermal Equilibrium.

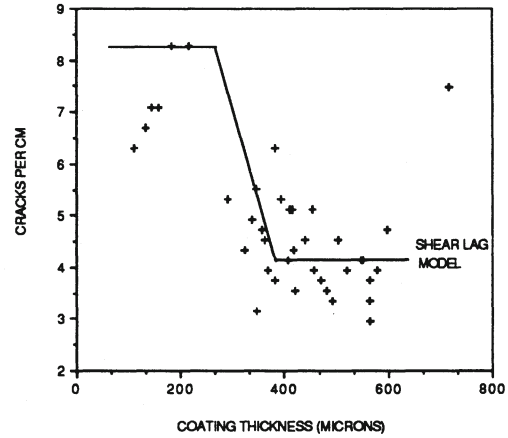

Fig. 6. Average Crack Spacing as a Function of Coating Thickness.

function of coating thickness and some experimental values are plotted for comparison. The experimental results, showing a broad trend of decreasing crack spacing with decreasing coating thickness, were in general agreement with the theoretical predictions. The wide degree of scatter most likely results from specimen-to-specimen variability in coating properties, and point-to-point thickness variations within individual specimens, accompanied by slight difficulties in measuring crack spacing in the presence of high background noise. Note that metallography showed interfacial cracking which was not considered in the model, and this is likely to cause some discrepancies.

COATING THICKNESS MEASUREMENT

Because coating thickness has a significant effect on oxidation resistance, alternative NDE methods for measuring coating thickness were evaluated; these were X-ray computed tomography, eddy current, and beta backscatter.

Cross-sections of the coupons were imaged using a GE CT9800 medical body scanner. The maximum image resolution, approximately 500μm, is not sufficient to give a direct measure of coating thickness. However, there are several methods to obtain sub-resolution information [2]. In the analysis used here the peak CT number was plotted against the coating thickness determined by metallography (Fig. 7).

Beta backscatter measurements were made using a Betascope 2000 instrument (Twin Cities Testing) and a Strontium 90 source. The Strontium isotope, with 2.18 MeV electrons, provided useful backscattered count rates; these are shown plotted against the coating thickness in Fig. 8(a).

A standard lift-off eddy current technique with a probe frequency of 100kHz was used. This technique was also used by the manufacturer for target thickness verification. Fig. 8(b) shows that these results correlated well with actual thickness measurements.

SUMMARY AND CONCLUSIONS

The differential absorption method could detect surface coating cracks, and contrast was improved by encapsulation of the fluorescent dye. Both coating thickness and oxidation state affected the crack patterns, and

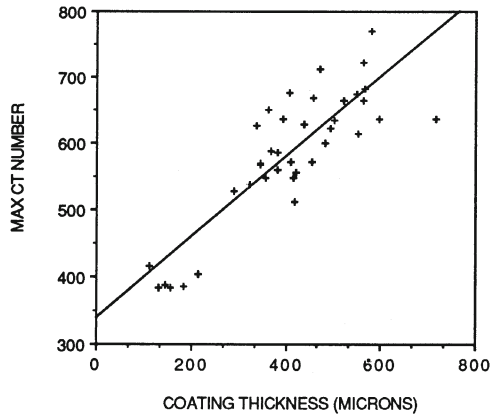

Fig. 7. Measurement of Coating Thickness from CT Cross-section.

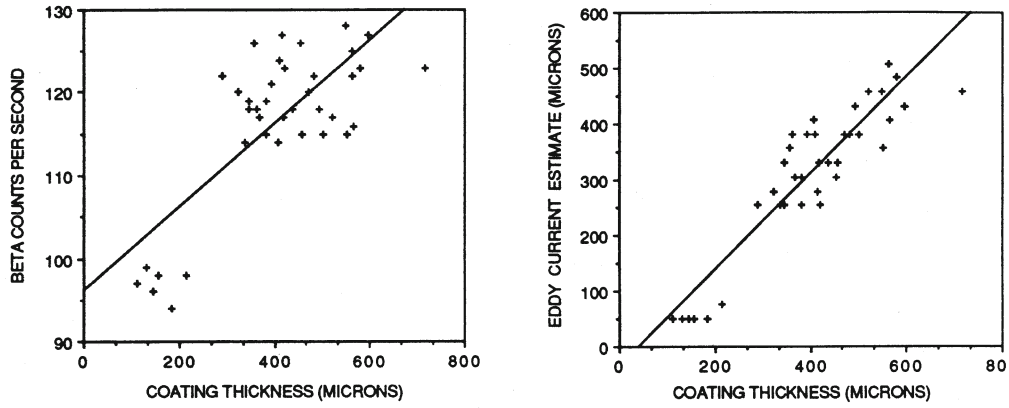

(a) Beta Backscatter (b) Eddy Current

Fig. 8. Correlation of Beta Backscatter and Eddy Current Measurements with Coating Thickness.

crack directions were normal to expected principal stress directions. Crack spacing varied with coating thickness in agreement with shear-lag calculations of thermal stresses.

Of the various alternative methods evaluated for measurement of coating thickness, the eddy current test proved most accurate, and has potential for improvement by using a multi-frequency approach to compensate for variability in substrate electrical conductivity. Computed tomography would also be useful where the surface may not be otherwise accessible.

ACKNOWLEDGEMENT

The work was sponsored by the Air Force Wright Aeronautical Laboratories Materials Laboratory under Contract Number F33615-84-C-5007.

REFERENCES

1. J.T. Olden and E.A. Rippenberger, in Mechanics of Elastic Structures (McGraw-Hill Book Company, 1983).
2. E. Segal, A. Notea, and Y. Segal, Materials Evaluation, Vol 40 (1982) p. 1268-1272.